Bull. Mater. Sci., Vol. 36, No. 4, August 2013, pp. 661–666. © Indian Academy of Sciences.

# Hydriding and dehydriding rates and hydrogen-storage capacity of Mg–14Ni–3$Fe_2O_3$–3Ti prepared by reactive mechanical grinding

**MYOUNG YOUP SONG[a,*], YOUNG JUN KWAK[b], HYE RYOUNG PARK[c] and BYOUNG-GOAN KIM[d]**

[a]Division of Advanced Materials Engineering, Hydrogen & Fuel Cell Research Center, Engineering Research Institute, Chonbuk National University, 664-14 Deokjin-Dong 1Ga Deokjin-Gu Jeonju Jeonbuk, 561-756, South Korea
[b]Department of Materials Engineering, Graduate School, Chonbuk National University, 664-14 Deokjin-Dong 1Ga Deokjin-Gu Jeonju Jeonbuk, 561-756, South Korea
[c]School of Applied Chemical Engineering, Chonnam National University, 300 Yongbong-Dong Buk-Gu Gwangju, 500-757, South Korea
[d]Korea Energy Materials Limited, 409 Daegu Technopark, 1-11 Hosan-Dong Dalse-Gu Daegu, 704-230, South Korea

MS received 20 October 2011; revised 5 February 2013

**Abstract.** **The magnesium prepared by mechanical grinding under $H_2$ (reactive mechanical grinding) with transition elements or oxides showed relatively high hydriding and dehydriding rates when the content of additives was about 20 wt%. Ni (expected to increase hydriding and dehydriding rates) was chosen as transition element to be added. $Fe_2O_3$ (expected to increase hydriding rate) was selected as an oxide to be added. Ti was also selected since, it was considered to increase the hydriding and dehydriding rates by forming Ti hydride. A sample, Mg–14Ni–3$Fe_2O_3$–3Ti, was prepared by reactive mechanical grinding and its hydrogen storage properties were investigated. This sample absorbed 4·02 wt% H for 5 min, 4·15 wt% H for 10 min and 4·42 wt% H for 60 min at $n = 2$. It desorbed 2·46 wt% H for 10 min, 3·98 wt% H for 30 min and 4·20 wt% H for 60 min at $n = 2$.**

**Keywords.** **Hydrogen absorbing materials; magnesium; reactive mechanical grinding; scanning electron microscopy; X-ray diffraction.**

## 1. Introduction

Hydrogen has been the focus of research and development efforts in the world. Hydrogen is believed to be able to meet the increasing demand for energy and decelerate global climate change. In fact, hydrogen can be produced from various sources such as fossil fuels, renewables and water by means of nuclear, wind, solar, tidal or geothermal energy. When hydrogen is converted into energy, water is the only exhaust product. It is thus extremely environmental friendly as an energy carrier.

Although hydrogen has obvious benefits, an immediate incorporation of hydrogen into the world economy has a number of difficulties to be solved. When compared to oil and natural gas, hydrogen has no large-scale infrastructure supporting its transportation. Hydrogen is largely used by chemical and refining industries. However, the cost of hydrogen storage and delivery is too high for much energy to be stored and transported using hydrogen as a major energy carrier.

The hydrogen economy infrastructure is made up of five key factors; production, delivery, storage, conversion and applications. While hydrogen production and conversion are technologically feasible, its delivery and storage face serious challenges.

There are several kinds of hydrogen storage methods; pressure storage, cryogenic storage, metal hydride storage, carbon nanotube storage, etc. Among these hydrogen storage methods, metal hydride storage can store more hydrogen per unit volume and is safer than pressure and cryogenic storages. To evolve hydrogen from the hydride, waste heat can be used. In addition, metal hydride absorbs and desorbs selectively hydrogen and thus, hydrogen with high purity can be produced.

Magnesium has a high hydrogen storage capacity (7·6 wt%), is of low cost and abundant in the earth's crust. However, its reaction rate with $H_2$ is very low (Vose 1961). A lot of work to improve the hydriding and dehydriding rates of magnesium has been performed by alloying magnesium with certain metals such as Cu (Reilly and Wiswall 1967), Ni (Reilly and Wiswall 1968; Akiba *et al* 1982), In (Mintz *et al* 1978), by synthesizing compounds such as $CeMg_{12}$ (Boulet and Gerard 1983) and $Mg_{76}Ti_{12}Fe_{12-x}Ni_x$ ($x = 4, 8$) (Lucaci *et al* 2009), and by making composites such as Mg–20 wt% $Fe_{23}Y_8$ (Li *et al* 2006), Mg–20 wt% Ni–Y (Li *et al* 2007), Mg–Sn (Zhong *et al* 2011) and Mg–V (Pei *et al* 2012). Aminorroaya *et al* (2011) added Nb and multi-walled carbon nanotubes to Mg–Ni alloys and Cho *et al* (2011)

*Author for correspondence (songmy@jbnu.ac.kr)

added transition metals to cast Mg–Ni alloys for improvement of the reaction rates of Mg with $H_2$. Milanese *et al* (2010) mixed Ni and Cu with Mg, Tanguy *et al* (1976) mixed metal additives with magnesium and Eisenberg *et al* (1980) plated nickel on the surface of magnesium to improve the hydriding–dehydriding kinetics of $MgH_2$.

The magnesium prepared by mechanical grinding under $H_2$ (reactive mechanical grinding) with transition elements or oxides showed relatively high hydriding and dehydriding rates when the content of the additives was about 20 wt%.

Reilly and Wiswall (1967) and Akiba *et al* (1982) improved the reaction kinetics of Mg with $H_2$ by preparing Mg–Ni alloys. Song *et al* (1985, 1987) and Song (1995a,b) increased the hydriding and dehydriding rates of Mg by mechanical alloying of Mg with Ni under Ar atmosphere. Bobet *et al* (2000) improved hydrogen-storage properties of both magnesium and Mg+10 wt% Co, Ni or Fe mixtures by reactive mechanical grinding for a short time (2 h). We chose Ni as a transition element to be added. Ti was also selected since it was considered to increase the hydriding and dehydriding rates when it was added. It forms Ti hydride, which can prevent magnesium from being agglomerated by staying as a hydride among Mg particles.

The oxides are brittle and thus they may be pulverized during mechanical grinding. The added oxides and/or their pulverization during mechanical grinding may help the particles of magnesium become finer, leading to increase in the hydriding and dehydriding rates of Mg. Addition of $Fe_2O_3$ prepared by spray conversion to Mg with reactive mechanical grinding improved greatly the hydriding rate of Mg (Song *et al* 2006). But the preparation of $Fe_2O_3$ by spray conversion is a complicated process. We thus used $Fe_2O_3$ to prepare the samples. Addition of too much $Fe_2O_3$ will decrease the hydrogen storage capacity. We added 3% to get a high effect of the oxide addition without decreasing the hydrogen storage capacity severely.

For these reasons, the content of additives was 20 wt% and we added Ni (expected to increase hydriding and dehydriding rates), $Fe_2O_3$ (as an oxide expected to increase hydriding rate) and Ti (expected to prevent agglomeration) in this work. We prepared samples with a composition of 80 wt% Mg–14 wt% Ni–3 wt% $Fe_2O_3$–3 wt% Ti by reactive mechanical grinding. The hydriding and dehydriding properties were then investigated. We designated 80 wt% Mg–14 wt% Ni–3 wt% $Fe_2O_3$–3 wt% Ti as Mg–14Ni–3$Fe_2O_3$–3Ti.

## 2. Experimental

Pure Mg powder (particle size, 297–100 $\mu$m, purity 99%, Fluka), Ni (average particle size ~5 $\mu$m, purity 99·9%, Cerac), $Fe_2O_3$ (average particle size <5 $\mu$m, purity ≥99%, Aldrich) and Ti (~44 $\mu$m, purity 99·9%, Aldrich) were used as starting materials.

Reactive mechanical grinding was done in a planetary ball mill (Planetary Mono Mill; Pulverisette 6, Fritsch). A mixture with the desired composition (total weight = 8 g) was mixed in a stainless steel container (with 105 hardened steel balls, total weight = 360 g) and sealed hermetically. The sample to ball weight ratio was 1/45. All sample handling was performed in a glove box under Ar in order to prevent oxidation. The disc revolution speed was 250 rpm. The mill container (volume, 250 ml) was then filled with high purity hydrogen gas (≈12 bar). The reactive mechanical grinding was performed for 6 h (milling 2 h + refilling with $H_2$ + milling 2 h + refilling with $H_2$ + milling 2 h). Pure Mg and Mg–10 wt% $Fe_2O_3$ samples were also prepared under similar conditions to investigate the effects of additives on the hydrogen-storage properties of Mg-based alloys.

The absorbed or desorbed hydrogen quantity was measured as a function of time by a volumetric method, using a Sievert's type hydriding and dehydriding apparatus described previously (Song *et al* 2010). 0·5 g of the samples was used for the measurement of the absorbed or desorbed hydrogen quantity as a function of time. X-ray diffraction (XRD) analysis was carried out for the as-milled powders and for the samples after hydriding–dehydriding cycling. The microstructures were observed by scanning electron microscopy (SEM).

## 3. Results and discussion

The percentage of absorbed hydrogen $H_a$ is expressed with respect to the sample weight. $H_a$ vs $t$ curve under 12 bar $H_2$ and $H_d$ vs $t$ curve under 1·0 bar $H_2$ at 573 K at $n = 1$ for Mg–14Ni–3$Fe_2O_3$–3Ti sample are presented in figure 1. The hydriding rate is very high from the beginning at about 10 min and thereafter it is extremely low. $H_a$ for 60 min can thus be considered as an effective hydrogen-storage capacity. The sample absorbs 3·15 wt% H for 2·5 min, 3·71 wt% H for 5 min, 3·89 wt% H for 10 min and 4·29 wt% H for 60 min. At the beginning, dehydriding rate of the sample is lower

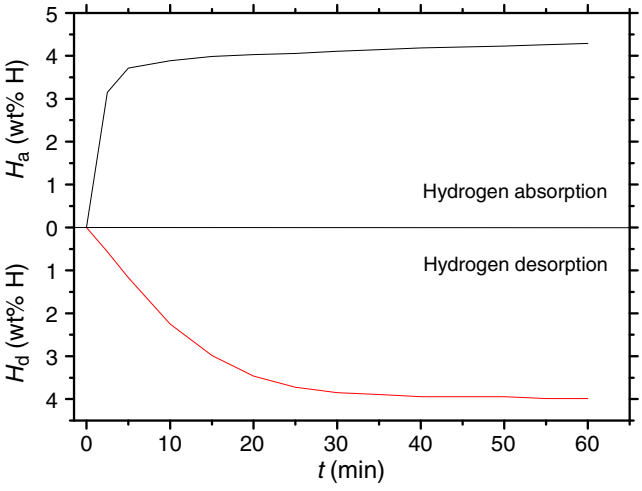


**Figure 1.** $H_a$ vs $t$ curve under 12 bar $H_2$ and $H_d$ vs $t$ curve under 1·0 bar $H_2$ at 573 K at $n = 1$ for Mg–14Ni–3$Fe_2O_3$–3Ti.

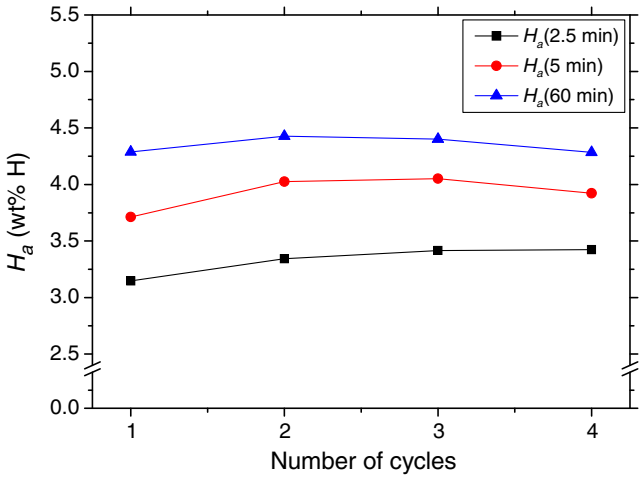


**Figure 2.** Variations of $H_a$(2·5 min), $H_a$(5 min) and $H_a$(60 min) with number of cycles at 573 K under 12 bar $H_2$ for Mg–14Ni–3Fe$_2$O$_3$–3Ti.

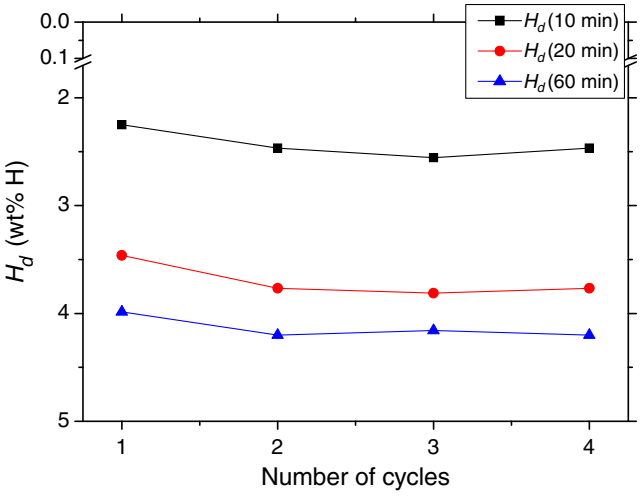


**Figure 3.** Variations of $H_d$(10 min), $H_d$(20 min) and $H_d$(60 min) with number of cycles at 573 K under 1·0 bar $H_2$ for Mg–14Ni–3Fe$_2$O$_3$–3Ti.

than its hydriding rate and $H_d$ varies linearly with time $t$ for about 10 min. The sample desorbs 0·56 wt% H for 2·5 min, 1·18 wt% H for 5 min, 2·49 wt% H for 10 min, 3·46 wt% H for 20 min, 3·85 wt% H for 30 min and 3·99 wt% H for 60 min.

The hydrogen quantities absorbed for 2·5, 5 and 60 min are expressed by $H_a$(2·5 min), $H_a$(5 min) and $H_a$(60 min), respectively. Figure 2 shows variations of $H_a$(2·5 min), $H_a$(5 min) and $H_a$(60 min) with the number of cycles at 573K under 12 bar $H_2$ for Mg–14Ni–3Fe$_2$O$_3$–3Ti. As the number of cycles increase from $n = 1$ to $n = 4$, $H_a$(2·5 min) increases. As the number of cycles increases from $n = 1$ to $n = 3$, $H_a$(5 min) increases and $t$ decreases from $n = 3$ to $n = 4$. As the number of cycles increases from $n = 1$ to $n = 2$, $H_a$(60 min) increases and it decreases from $n = 2$ to $n = 4$. This sample absorbs 3·34 wt% H for 2·5 min, 4·02 wt% H for 5 min, 4·15 wt% H for 10 min and 4·42 wt% H for 60 min at $n = 2$.

The variation of $H_d$(10 min), $H_d$(20 min) and $H_d$(60 min) with the number of cycles at 573K under 1·0 bar $H_2$ for Mg–14Ni–3Fe$_2$O$_3$–3Ti are shown in figure 3. As the number of cycles increases from $n = 1$ to $n = 3$, $H_d$(10 min) and $H_d$(20 min) increase and they decrease from $n = 3$ to $n = 4$. As the number of cycles increases from $n = 1$ to $n = 2$, $H_d$(60 min) increases and it decreases from $n = 2$ to $n = 3$. The values of $H_d$(60 min) are similar at $n$ =2–4. This sample desorbs 2·46 wt% H for 10 min, 3·77 wt% H for 20 min, 3·98 wt% H for 30 min and 4·20 wt% H for 60 min at $n = 2$.

At $n$=2, Mg–14Ni–3Fe$_2$O$_3$–3Ti sample absorbs 4·42 wt% H, but desorbs 4·20 wt% H for 60 min. The sample was dehydrided under 1·0 bar $H_2$ and the dehydriding reaction continues even after 60 min. It is believed that more hydrogen would be released if the dehydriding reaction measurement was performed for more than 60 min or if it was dehydrided in vacuum.

The results in figures 2 and 3 show that activation of Mg–14Ni–3Fe$_2$O$_3$–3Ti sample is completed after the first hydriding–dehydriding cycle.

Figure 4 exhibits microstructure of Mg–14Ni–3Fe$_2$O$_3$–3Ti after reactive mechanical grinding at different magnifications. The sample has small particles and agglomerated large particles.

The microstructure of Mg–14Ni–3Fe$_2$O$_3$–3Ti after hydriding–dehydriding ($n = 4$) at different magnifications is shown in figure 5. The sample also has small particles and agglomerated large particles. This sample has particles similar to those after reactive mechanical grinding, but the small particles are finer than those in the sample after reactive mechanical grinding.

XRD pattern of Mg–14Ni–3Fe$_2$O$_3$–3Ti after reactive mechanical grinding contained Ni, $MgH_2$, Mg and $Fe_2O_3$. $MgH_2$ was formed by the reaction of Mg with hydrogen during reactive mechanical grinding.

Figure 6 illustrates XRD pattern of dehydrided Mg–14Ni–3Fe$_2$O$_3$–3Ti after hydriding–dehydriding cycling ($n = 4$). The sample contains Mg, $Mg_2Ni$, $MgH_2$ and MgO. This shows that $Mg_2Ni$ is formed by the reaction of Mg with Ni during hydriding–dehydriding cycling. The formation of $Mg_2Ni$ phase, which has higher hydriding and dehydriding rates than Mg, is believed to increase the hydriding and dehydriding rates of Mg. A research grade high purity hydrogen was used, but a extremely small amount of impurity in hydrogen is believed to have led to the formation of MgO.

Figure 7 shows BET graphs [$1/\{V_a(P_0/P - 1)\}$ vs $P/P_0$ plots] for Mg–14Ni–3Fe$_2$O$_3$–3Ti after reactive mechanical grinding and activation, where $V_a$ is the volume of adsorbed gas, $P_0$ the saturated pressure of adsorbed gas and $P$ the equilibrium pressure of adsorbed gas. According to BET equation, the specific surface area is large when plot $1/\{V_a(P_0/P - 1)\}$ vs $P/P_0$ has a small slope and a small

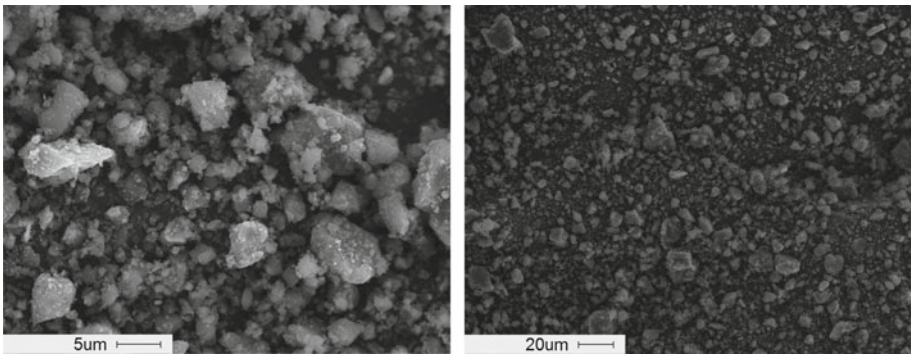


**Figure 4.** Microstructure of Mg–14Ni–3$Fe_2O_3$–3Ti after reactive mechanical grinding at different magnifications.

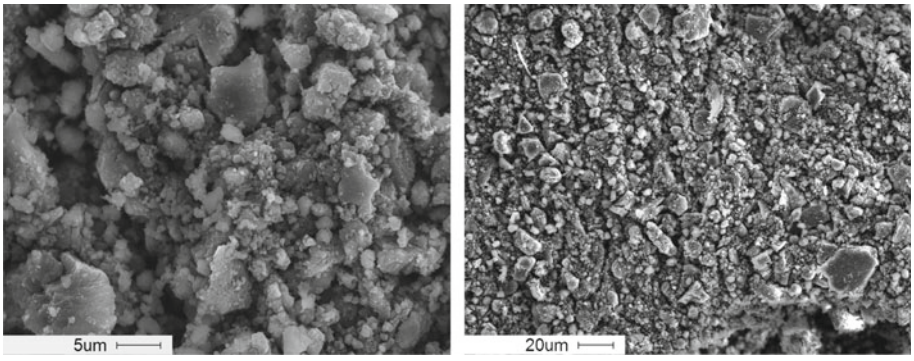


**Figure 5.** Microstructure of Mg–14Ni–3$Fe_2O_3$–3Ti after hydriding–dehydriding ($n = 4$) at different magnifications.

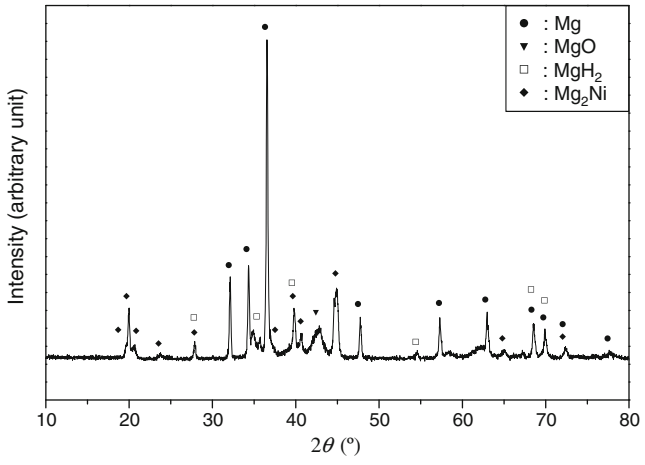


**Figure 6.** XRD pattern of dehydrided Mg–14Ni–3$Fe_2O_3$–3Ti after hydriding–dehydriding cycling ($n = 4$).

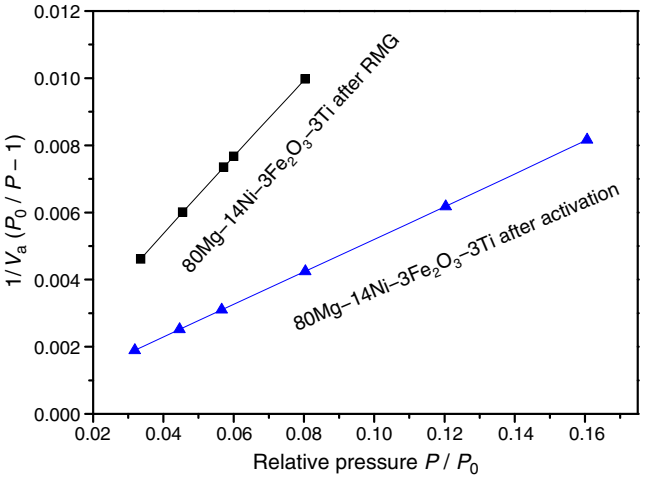


**Figure 7.** BET graphs ($1/\{V_a(P_0/P - 1)\}$ vs $P/P_0$ plots) for Mg–14Ni–3$Fe_2O_3$–3Ti after reactive mechanical grinding and activation.

value of intercept on the vertical axis. Mg–14Ni–3$Fe_2O_3$–3Ti samples after reactive mechanical grinding and activation have specific surface areas of 37·8 and 88·9 $m^2/g$, respectively. On an assumption that the particles are spherical and their sizes are homogeneous and that the sample is composed mainly of Mg, their sizes were calculated as 30·5 and 13·0 nm, respectively from an equation of particle size (m) = 6/[{specific surface area ($m^2/g$)} × density, 5·21 × $10^6$ $g/m^3$]. The specific surface area of the sample increases after activation, probably due to expansion and contraction with hydriding and dehydriding reactions which lead to crack formation and decrease in the particle size.

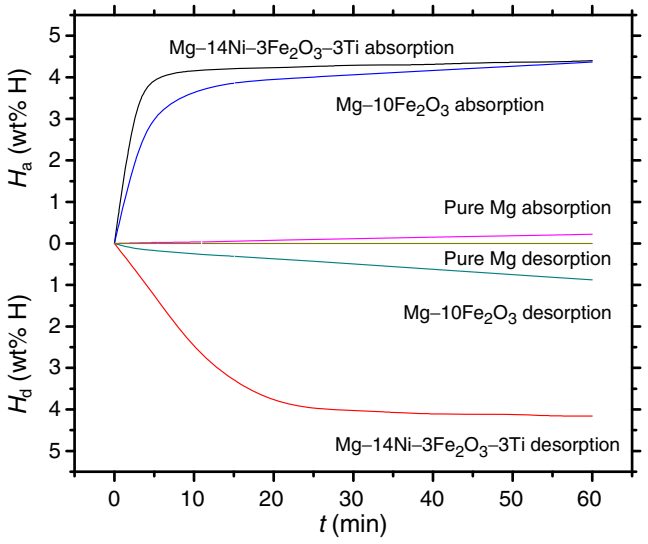


**Figure 8.** $H_a$ vs $t$ curves under 12 bar $H_2$ at $n = 3$ for activated Mg–10$Fe_2O_3$ (at 573 K), Mg–14Ni–3$Fe_2O_3$–3Ti (at 573 K) and pure Mg (at 593 K) and $H_d$ vs $t$ curves under 1·0 bar $H_2$ at $n = 3$ for activated Mg–10$Fe_2O_3$ (at 593 K), Mg–14Ni–3$Fe_2O_3$–3Ti (at 573 K) and pure Mg (at 593 K).

Figure 8 shows $H_a$ vs $t$ curves under 12 bar $H_2$ at $n = 3$ for activated Mg–10$Fe_2O_3$ (at 573 K), Mg–14Ni–3$Fe_2O_3$–3Ti (at 573 K) and pure Mg (at 593 K), and $H_d$ vs $t$ curves under 1·0 bar $H_2$ at $n = 3$ for activated Mg–10$Fe_2O_3$ (at 593 K), Mg–14Ni–3$Fe_2O_3$–3Ti (at 573 K) and pure Mg (at 593 K). $H_a$ value for the activated pure Mg increases linearly with time. The activated pure Mg absorbs hydrogen very slowly at 593 K under 12 bar $H_2$. It absorbs 0·02 wt% H for 5 min, 0·03 wt% H for 10 min and 0·22 wt% H for 60 min. The activated pure Mg does not desorb hydrogen at 593 K under 1·0 bar $H_2$. Due to the addition of $Fe_2O_3$, the hydriding rate is greatly increased while the dehydriding rate is slightly increased. The activated Mg–10$Fe_2O_3$ absorbs 3·18 wt% H for 5 min, 3·69 wt% H for 10 min and 4·37 wt% H for 60 min. The activated Mg–10$Fe_2O_3$ desorbs 0·17 wt% H for 5 min, 0·26 wt% H for 10 min and 0·88 wt% H for 60 min. The activated Mg–14Ni–3$Fe_2O_3$–3Ti has higher hydriding and much dehydriding rates than the activated Mg–10$Fe_2O_3$ and the activated pure Mg.

The sample prepared by reactive mechanical grinding is a physical mixture, but the components of the mixture are well mixed and particles of the components are well contacted. During milling under $H_2$, $MgH_2$ was formed and after hydriding–dehydriding cycling, $Mg_2Ni$ was formed.

The results in figure 8 show that reactive mechanical grinding of Mg with Ni, $Fe_2O_3$ and Ti increases the hydriding and dehydriding rates of Mg.

Song (1995a) reviewed the kinetic studies of hydriding and dehydriding reactions of Mg. Many works do not agree with one another on the rate-controlling step(s) for hydriding or dehydriding of magnesium. However, there is consensus in the points that the hydriding and dehydriding reactions of Mg are nucleation-controlled under certain conditions and progress by a mechanism of nucleation and growth and that the hydriding rates of Mg are controlled by the diffusion of hydrogen through a growing Mg hydride layer.

The reactive mechanical grinding of Mg with Ni, $Fe_2O_3$ and Ti is considered to facilitate nucleation by creating many defects on the surface and/or in the interior of Mg, or by the additives acting as active sites for the nucleation and shorten diffusion distances of hydrogen atoms by reducing the particle size of Mg.

Created defects and cracks and the fragmentation into fine particles, due to the expansion and contraction of the hydride-forming materials (Mg and $Mg_2Ni$) with the hydriding and dehydriding reactions are also considered to increase the higher hydriding and dehydriding rates of the alloys.

Figure 8 shows that the addition of $Fe_2O_3$ increases greatly the hydriding rate of Mg and slightly the dehydriding rate of $MgH_2$. $Mg_2Ni$ has higher hydriding and dehydriding rates than Mg. Figure 6 shows that $Mg_2Ni$ is formed in Mg–14Ni–6$Fe_2O_3$ sample after hydriding–dehydriding cycling. The addition of $Fe_2O_3$ increased slightly the dehydriding rate of $MgH_2$ while Mg–14Ni–6$Fe_2O_3$ sample has quite high dehydriding rate. This proves that the addition of Ni increases greatly the dehydriding rate of $MgH_2$. The addition of Ni increases the hydriding rate of Mg as well as the dehydriding rate of $MgH_2$ by the formation of $Mg_2Ni$ from the reaction of Ni with Mg during hydriding–dehydriding cycling.

We also measured the hydriding and dehydriding rates of the samples with compositions of Mg–14Ni–6$Fe_2O_3$ and Mg–14Ni–2$Fe_2O_3$–2Ti–2Fe prepared under the same conditions. Among these compositions, Mg–14Ni–3$Fe_2O_3$–3Ti had the best hydrogen-storage properties.

## 4. Conclusions

A sample, Mg–14Ni–3$Fe_2O_3$–3Ti, was prepared by reactive mechanical grinding and its hydrogen-storage properties were examined. The activation of the as-milled Mg–14Ni–3$Fe_2O_3$–3Ti sample was completed after the first hydriding–dehydriding cycle. At $n = 2$, this sample absorbed 4·02 wt%, H for 5 min, 4·15 wt% H for 10 min and 4·42 wt% H for 60 min, which can be considered as an effective hydrogen-storage capacity. It desorbed 2·46 wt% H for 10 min, 3·98 wt% H for 30 min and 4·20 wt% H for 60 min at $n = 2$. During reactive mechanical grinding, $MgH_2$ was formed by the reaction of Mg with hydrogen. The dehydrided Mg–14Ni–3$Fe_2O_3$–3Ti after hydriding–dehydriding cycling contained Mg, $Mg_2Ni$, $MgH_2$ and MgO. The addition of $Fe_2O_3$ increased greatly the hydriding rate of Mg and slightly the dehydriding rate of $MgH_2$. The addition of Ni increases hydriding rate of Mg as well as dehydriding rate of $MgH_2$ by the formation of $Mg_2Ni$ from the reaction of Ni with Mg during hydriding–dehydriding cycling.

**Acknowledgement**

This research was performed for Hydrogen Energy R&D Centre, one of the 21st Century Frontier R&D Programs funded by Ministry of Science and Technology.

**References**

Akiba E, Nomura K, Ono S and Suda S 1982 *Int. J. Hydrogen Energy* **7** 787

Aminorroaya S, Ranjbar A, Cho Y H, Liu H K and Dahle A K 2011 *Int. J. Hydrogen Energy* **36** 571

Bobet J-L, Akiba E, Nakamura Y and Darriet B 2000 *Int. J. Hydrogen Energy* **25** 987

Boulet J M and Gerard N 1983 *J. Less-Common Met.* **89** 151

Cho Y H, Aminorroaya S, Liu H K and Dahle A K 2011 *Int. J. Hydrogen Energy* **36** 4984

Eisenberg F G, Zagnoli D A and Sheridan III J J 1980 *J. Less-Common Met.* **74** 323

Li Z, Liu X, Huang Z, Jiang L and Wang S 2006 *Rare Metals* **25** 247

Li Z, Liu X, Jiang L and Wang S 2007 *Int. J. Hydrogen Energy* **32** 1869

Lucaci M, Biris A R, Orban R L, Sbarcea G B and Tsakiris V 2009 *J. Alloys Compd.* **488** 163

Milanese C, Girella A, Bruni G, Cofrancesco P, Berbenni V, Matteazzi P and Marini A 2010 *Intermetallics* **18** 203

Mintz M H, Gavra Z and Hadari Z (1978) *J. Inorg. Nucl. Chem.* **40** 765

Pei P, Song X, Liu J, Song A, Zhang P and Chen G 2012 *Int. J. Hydrogen Energy* **37** 984

Reilly J J and Wiswall R H 1967 *Inorg. Chem.* **6** 2220

Reilly J J and Wiswall Jr R H 1968 *Inorg. Chem.* **7** 2254

Song M Y 1995a *J. Mater. Sci.* **30** 1343

Song M Y 1995b *Int. J. Hydrogen Energy* **20** 221

Song M Y, Ivanov E I, Darriet B, Pezat M and Hagenmuller P 1985 *Int. J. Hydrogen Energy* **10** 169

Song M Y, Ivanov E I, Darriet B, Pezat M and Hagenmuller P 1987 *J. Less-Common Met.* **131** 71

Song M Y, Kwon I H, Kwon S N, Park C G, Hong S H, Mumm D R and Bae J S 2006 *J. Alloys Compd.* **415** 266

Song M Y, Baek S H, Bobet J-L and Hong S H 2010 *Int. J. Hydrogen Energy* **35** 10366

Tanguy B, Soubeyroux J L, Pezat M, Portier J and Hagenmuller P 1976 *Mater. Res. Bull.* **11** 1441

Vose A 1961 *Metal hydrides*, U.S. Patent 2,944,587

Zhong H C, Wang H, Ouyang L Z and Zhu M 2011 *J. Alloys Compd.* **509** 4268